Discrete surface solitons in two dimensions

H. Susanto,[1] P. G. Kevrekidis,[1] B. A. Malomed,[2] R. Carretero-González,[3] and D. J. Frantzeskakis[4]
[1]*Department of Mathematics and Statistics, University of Massachusetts, Amherst, Massachusetts 01003-4515, USA*
[2]*Department of Interdisciplinary Studies, School of Electrical Engineering, Faculty of Engineering, Tel Aviv University, Tel Aviv 69978, Israel*
[3]*Nonlinear Dynamical Systems Group, Department of Mathematics and Statistics, and Computational Science Research Center, San Diego State University, San Diego, California, 92182-7720, USA*
[4]*Department of Physics, University of Athens, Panepistimiopolis, Zografos, Athens 15784, Greece*
(Received 26 July 2006; revised manuscript received 28 February 2007; published 9 May 2007)

We investigate fundamental localized modes in two-dimensional lattices with an edge (surface). The interaction with the edge expands the stability area for fundamental solitons, and induces a difference between dipoles oriented perpendicular and parallel to the surface. On the contrary, lattice vortex solitons cannot exist too close to the border. We also show, analytically and numerically, that the edge supports a species of localized patterns, which exists too but is unstable in the uniform lattice, namely, a horseshoe-shaped soliton, whose "skeleton" consists of three lattice sites. Unstable horseshoes transform themselves into a pair of ordinary solitons.

DOI: 10.1103/PhysRevE.75.056605 PACS number(s): 05.45.Yv, 03.75.−b, 42.65.Tg

I. INTRODUCTION AND THE MODEL

Solitons on surfaces of fluids [1], solids [2], and plasmas [3] have been the subject of many experimental and theoretical studies for a long time. Recently, a implementation of surface solitary waves was proposed [4] and experimentally realized [5] in nonlinear optics, in the form of discrete localized states formed at the edge of a semi-infinite array of nonlinear waveguides. If the nonlinearity in the semi-infinite array of the waveguides is self-defocusing, the surface solitons demonstrate a staggered (sign-alternating) shape, as shown experimentally and theoretically in Ref. [6]. Very recently, it was demonstrated that hybrid solitons at an interface between two lattices are possible too, with a shape which is unstaggered on one side of the interface, and staggered on the other [7]. Two-component surface solitons were analyzed as well, in a model with the nonlinear coupling between the components [8], and it was predicted that solitons may be supported at an edge of a discrete chain by a nonlinear impurity (i.e., assuming the coefficient of the onsite cubic nonlinearity at the last site of the chain different from that at other sites) [9]. Parallel to that, surface solitons of the gap type were predicted [10] and created in an experiment [11] at an edge of a waveguide array built into in a self-defocusing continuous medium. Very recently, experimental creation of discrete surface solitons supported by the quadratic nonlinearity was reported as well [12].

In the abovementioned cases, the solitons are one-dimensional (1D) objects. Two-dimensional (2D) lattices with an edge may be considered too. If the lattice is realized as a 2D array (bundle) of optical waveguides, the edge corresponds to a surface running parallel to the waveguides that form the lattice. In particular, in Ref. [13], a 2D medium was considered, with saturable nonlinearity and an embedded square lattice, an internal surface in the medium being introduced by a jump of the refractive index; in this setting, stable asymmetric vortex solitons crossing the interface were predicted, as a generalization of discrete vortices on 2D lattices [14] and vortex solitons supported by optically induced lattices in photorefractive media [15]. Solitons supported by a nonlinear defect at the edge of a 2D lattice were considered too [16].

The search for surface solitons in lattice settings is a natural direction of the research, as, in any experimental setup, the lattice inevitably has an edge. In this paper, we report results for discrete surface solitons in semi-infinite 2D lattices. First, we consider the effect of the surface on fundamental lattice solitons, and two types of dipoles, oriented perpendicular or parallel to the surface. Then, we introduce a novel species of localized states, a horseshoe soliton, in the form of an arc abutting upon the lattice's edge. The existence, and especially the stability, of such a localized mode is a nontrivial issue, as attempts to find a "horseshoe" in continuum media with imprinted lattices and an internal interface (such as those considered in Ref. [13]) have produced negative results [17]. We find that, in the semi-infinite discrete medium, the horseshoes do exist near the lattice edge, and possess a stability region. For comparison, we also construct a family of localized patterns of the same type in the uniform lattice [which, incidentally, is a kind of a stationary localized solution of the 2D discrete nonlinear Schrödinger (DNLS) equation, that has not been studied previously]. In particular, we find that this family of solutions is always unstable in the infinite uniform lattice (the one without an edge), which stresses the nontrivial character of the surface-abutting horseshoes, that may be made stable by the interaction with the lattice edge.

The model of the abovementioned semi-infinite 2D array of optical waveguides with a horizontal edge, whose plane is parallel to the waveguides (which is a physically relevant representation of 2D lattices bounded by a flat surface), is based on the DNLS equation for amplitudes $u_{m,n}(z)$ of the electromagnetic waves in the guiding cores, with z being the propagation distance:

$$i\frac{du_{m,n}}{dz} + C(u_{m+1,n} + u_{m-1,n} + u_{m,n+1} + u_{m,n-1} - 4u_{m,n}) + |u_{m,n}|^2 u_{m,n} = 0, \quad (1)$$

for $n \geqslant 2$ and any m, while C is the coupling constant; note that the corresponding coupling length in the waveguide array, C^{-1}, is usually on the order of a few millimeters, in physical units. At the surface row, which corresponds to $n=1$ in Eq. (1), the equation is modified by dropping the fourth term in the combination of linear terms in Eq. (1) (cf. the 1D model introduced in Refs. [5]), $u_{m,0}=0$, as there are no waveguides at $n \leqslant 0$. Note that, despite the presence of the edge, Eq. (1) admits the usual Hamiltonian representation, and conserves the total power (norm), $P=\Sigma_{m=-\infty}^{+\infty}\Sigma_{n=1}^{+\infty}|u_{m,n}|^2$.

There is another physical realization of the same model. Indeed, DNLS equation (1) describes, in the mean-field approximation, the dynamics of a Bose-Einstein condensate (BEC) trapped in a strong 2D optical lattice [18] (the latter is a periodic potential induced by the interference of counterpropagating pairs of coherent laser beams illuminating the condensate). In such a case, $u_{m,n}$ is the condensate wave function, and C is the rate of tunneling between adjacent wells in the optical lattice. Notice that a sharp edge in BEC can be created by a repelling (blue-detuned) light sheet.

Stationary solutions to Eq. (1) will be looked for as $u_{m,n}=e^{ikz}v_{m,n}$, where the wave number k may be scaled to 1, once the coupling coefficient C is kept as an arbitrary parameter. The above stationary solution obeys the equation

$$f(v_{m,n},\bar{v}_{m,n},C) = (1-|v_{m,n}|^2)v_{m,n} - C(v_{m,n+1} + v_{m,n-1} + v_{m+1,n} + v_{m-1,n} - 4v_{m,n}) = 0, \quad (2)$$

with the same modification as above at $n=1$ (the overbar will be used to denote complex conjugation). Notice that the solution also satisfies the complex conjugate equation $\bar{f}(v_{m,n},\bar{v}_{m,n},C)=0$.

The rest of the paper is organized as follows. In Sec. II, we report results obtained by means of an analytical approximation for the shape and stability of dipoles and "horseshoes," valid for a weakly coupled lattice (small C), which is followed by presentation of corresponding numerical results. In Sec. III we briefly consider the interaction of vortices with the lattice's edge. Finally, our findings are summarized in Sec. IV.

II. FUNDAMENTAL SOLITONS, DIPOLES, AND HORSESHOES

A. Analytical approach

Analytical results can be obtained for small C, starting from the anticontinuum (AC) limit $C=0$ (see Ref. [19], and references therein). In this case, solutions to Eq. (2) are constructed using the expansion

$$v_{m,n} = \sum_{k=0}^{\infty} C^k v_{m,n}^{(k)}.$$

In the ac limit proper, the seed solution $v_{m,n}^{(0)}$ is zero except at a few excited sites, which determine the configuration. While a great variety of seed solutions may be formally constructed at $C=0$, a nontrivial issue is to identify solutions that can be continued to finite values of C, an even more important question being which ones among them are stable. As concerns the experimental realization, the necessary set of sites can be easily excited selectively, by focusing the input laser beam(s) on them, as shown, for instance, in experimental studies of interactions between discrete solitons in waveguide arrays [20].

We will present analytical results for the following configurations, which are selected as ones bearing a minimum necessary number of excited sites in the ac limit: (A) a fundamental surface soliton, seeded by a single excited site $v_{0,1}^{(0)}=1$, (B) surface dipoles, oriented perpendicular (B1) or parallel (B2) to the edge, each seeded at two sites

$$\{v_{0,1}^{(0)}, v_{0,2}^{(0)}\} = \{-1,1\} \quad \text{or} \quad \{v_{0,1}^{(0)}, v_{1,1}^{(0)}\} = \{-1,1\}, \quad (3)$$

and (C) the horseshoe-shaped three-site-seeded structure

$$\{v_{1,1}^{(0)}, v_{0,2}^{(0)}, v_{-1,1}^{(0)}\} = \{e^{i\theta_{1,1}}, e^{i\theta_{0,2}}, e^{i\theta_{-1,1}}\}, \quad (4)$$

with $\theta_{1,1}=0$, $\theta_{0,2}=\pi$, $\theta_{-1,1}=2\pi$. As concerns stable dipole states on the infinite lattice, they were predicted in Ref. [21], and later observed experimentally in a photonic lattice induced in a photorefractive crystal [22]. All the above seed configurations are real; in particular, the horseshoe may, in principle, be regarded as a truncated quadrupole, which is a real solution too [23].

At small $C>0$, it is straightforward to continue the stationary solutions at the first order in C. Then, one has to address the issue of stability which in this work we examine at the level of linear stability analysis.

The linearization operator for the two difference equations $f(v_{m,n},\bar{v}_{m,n},C)$ and $\bar{f}(v_{m,n},\bar{v}_{m,n},C)$ reads

$$\mathcal{H}_{n,m} = \begin{pmatrix} 1-2|v_{n,m}|^2 & -v_{n,m}^2 \\ -\bar{v}_{n,m}^2 & 1-2|v_{n,m}|^2 \end{pmatrix} - C(s_{+1,0}+s_{-1,0}+s_{0,+1}+s_{0,-1}) \begin{pmatrix} 1 & 0 \\ 0 & 1 \end{pmatrix}, \quad (5)$$

where $s_{n',m'}v_{n,m}=v_{n+n',m+m'}$. Then, according to the theory of Ref. [19], the solvability condition (allowing us to continue a solution valid for $C=0$ to nonzero values of the coupling) necessitates that the projection of the eigenvectors of the kernel of $\mathcal{H}_{n,m}^{\epsilon=0}$ to the Eq. (2) and its conjugate is null. The theory developed in Ref. [19] directly links this bifurcation condition, to be called $g_j(\theta_j)$ for each excited site j of the configuration, to the linear stability problem. In particular, computing the Jacobian matrix pertaining to these bifurcation conditions $(\mathcal{M})_{j,k} \equiv \partial g_j / \partial \theta_k$, one can immediately compute the leading-order behavior of eigenvalues of the linearization according to the explicit formula

$$\lambda = \sqrt{2C\mu}, \quad (6)$$

where μ denotes the eigenvalues of the matrix $\mathcal{M}$ (we note in passing that if the excited sites are more than one site apart, then the order of the power of C in the above expression needs to be accordingly modified to higher powers of $\sqrt{C}$; see for details Ref. [19] and as an example the second

order construction of the horseshoe configuration below). Therefore, the analytical results obtained below have been constructed by first extracting g_j, then computing the Jacobian $\mathcal{M}$, subsequently finding its eigenvalues μ, and finally using Eq. (6) to find the leading order behavior of the linear stability eigenvalues λ of the original problem. Because the present system is a Hamiltonian one, the stability condition $\mathrm{Re}(\lambda)=0$ must hold for all λ (if λ is an eigenvalue, so are also $-\lambda$, $\lambda^\star$ and $-\lambda^\star$, hence only purely imaginary λ does not imply instability).

For the dipole and horseshoe configurations, which were denoted above as (B1), (B2), and (C), respectively, the calculations result in the following bifurcation functions:

$$g_1^{(\mathrm{B})} = \sin(\theta_1 - \theta_2),$$

$$g_2^{(\mathrm{B})} = \sin(\theta_2 - \theta_1),$$

where θ_1 represents $\theta_{0,1}$ and θ_2 denotes $\theta_{0,2}$ for configuration B1 and $\theta_{1,1}$ for B2, and

$$g_1^{(\mathrm{C})} = 2\sin(\theta_1 - \theta_3) + 2\sin(\theta_1 - \theta_2),$$

$$g_2^{(\mathrm{C})} = 2\sin(\theta_2 - \theta_1) + \sin(\theta_2 - \theta_3),$$

$$g_3^{(\mathrm{C})} = 2\sin(\theta_3 - \theta_1) + \sin(\theta_3 - \theta_2),$$

with $\theta_1=\theta_{0,2}$, $\theta_2=\theta_{-1,1}$, and $\theta_3=\theta_{1,1}$.

The bifurcation equations above give the following Jacobian stability matrices:

$$\mathcal{M}^{(\mathrm{B})} = C\begin{pmatrix} -1 & 1 \\ 1 & -1 \end{pmatrix} + O(C^2),$$

$$\mathcal{M}^{(\mathrm{C})} = C^2\begin{pmatrix} -4 & 2 & 2 \\ 2 & -1 & -1 \\ 2 & -1 & -1 \end{pmatrix} + O(C^3)$$

[the matrices for (B1) and (B2) coincide at this order]. From here, we obtain *stable* eigenvalues, at the lowest nontrivial order:

$$\lambda_1^{(\mathrm{B})} = 0, \quad \lambda_2^{(\mathrm{B})} = \pm 2\sqrt{C}i + O(C), \tag{7}$$

and

$$\lambda_1^{(\mathrm{C})} = 0, \quad \lambda_2^{(\mathrm{C})} = O(C^2),$$

$$\lambda_3^{(\mathrm{C})} = \pm 2\sqrt{3C}i + O(C^2). \tag{8}$$

For both the dipoles and horseshoe, one eigenvalue is exactly zero, corresponding to the Goldstone mode generated by the phase invariance of the underlying DNLS equation. It is shown below that eigenvalue $\lambda_2^{(\mathrm{C})}$, which is different from zero at order C^2, plays a critical role in determining the stability of the horseshoe structure.

B. Numerical results

To examine the existence and stability of the localized configurations numerically, we start with the fundamental onsite soliton at the surface (A) [we did not apply the analytical method to this solution, as its actual destabilization mechanism is different (and requires a different analysis) from that for the dipoles and horseshoes; in particular, the critical eigenvalues bifurcate not from zero, but from the edge of continuous spectrum, see below]. Basic results for this state are displayed in Fig. 1. At $C=0$, there is a zero eigenvalue pair due to the phase invariance. For small $C>0$, this is the only eigenvalue located near the origin of the spectral plane $[\mathrm{Re}(\lambda),\mathrm{Im}(\lambda)]$. As C increases, one encounters a critical value of the coupling constant, at which an additional (but still marginally stable) eigenvalue bifurcates from the edge of the continuous spectrum. The continuous spectrum of linear excitations, given by the known dispersion relation $\lambda=\pm i\{\Lambda+C[4-2\cos(k_x)-2\cos(k_y)]\}$ for linear waves with wave numbers (k_x,k_y), covers the interval $\pm i[\Lambda,\Lambda+4C]$ (alias the phonon band) [24]. Upon further increase of C, the bifurcating eigenvalue hits the origin of the spectral plane, thus giving birth to an unstable real eigenvalue pair, with $\mathrm{Re}(\lambda)\neq 0$, see panel (c) in Fig. 1. The corresponding instability occurs at $C>1.41$ (the results reported here have been obtained for the lattice of size 10×10, but it has been verified that a similar situation persists for larger lattices, up to the maximum size that was used in the computations, 25×25). For comparison, Fig. 1 also displays, by a dashed-dotted line, the critical unstable eigenvalue for a fundamental soliton on the uniform lattice (in other words, for a soliton sitting far from the lattice's edge), which demonstrates that the interaction with the edge leads to a conspicuous expansion of the stability interval of the fundamental soliton. This result may be understood, as the instability of the fundamental soliton emerges as one approaches the continuum limit; 2D solitons in the continuum NLS equation are well known to be unstable due to the possibility of the collapse or dispersion in that case. On the other hand, a discrete fundamental soliton located near the surface interacts with fewer neighboring sites, hence it approaches the continuum limit slower, in comparison with its counterpart in the infinite lattice, and will become unstable for larger values of C; however, in any case the fundamental soliton eventually becomes unstable against quasicollapse (see e.g., Ref. [25], and references therein) or dispersion. By the term "quasicollapse," we mean the lattice analog of the collapse development in the continuum: given the conservation of power P, in a lattice setting it is not possible to have divergence of the amplitude $\max_n(|u_n(t)|)\to\infty$, as the amplitude is bounded, according to $\max_n(|u_n(t)|)<\sqrt{P}$. Hence, the closest analog to collapse that a dynamical lattice can exhibit is the concentration of nearly all of its power at a single site, which is the extreme manifestation of the quasicollapse.

Development of the instability of the fundamental surface soliton (in the case when it is unstable) was examined in direct simulations of Eq. (1). As seen in panel (d) of Fig. 1, in this case the soliton moves away from the lattice's edge, expanding into an apparently disordered state (lattice radiation). This outcome of the instability development is understandable, as, at these values of the parameters, no stable localized state exists, neither near the surface nor in the bulk of the lattice (where the fundamental soliton is still more unstable).

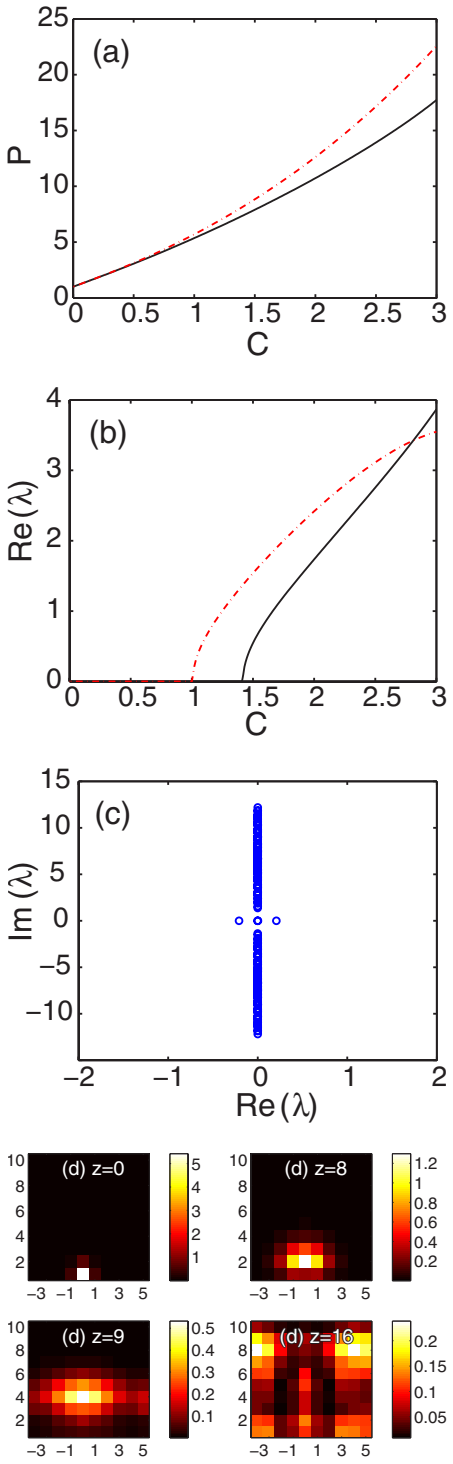

FIG. 1. (Color online) Dynamical features of the family of fundamental lattice-surface solitons: (a) norm P and (b) the real part of the critical stability eigenvalue, versus the lattice coupling constant C. For comparison, the dashed-dotted lines show respective quantities for the fundamental soliton in the infinite lattice. The instability is due to an eigenvalue pair bifurcating from the edge of the phonon band, that eventually hits the origin of the spectral plane and thus becomes real. (c) Linear-stability spectrum of the fundamental soliton for $C=1.43$. (d) Snapshots of its evolution (contour plots of $|u_{m,n}|^2$), slightly above the instability threshold (at $C=1.43$).

Next, in Fig. 2 we present numerical results for the vertical and horizontal dipoles (B1) and (B2) seeded as per Eq. (3). Recall that, at $C=0$, the spectrum of the eigenmodes found by means of the perturbative approach around the dipole, see Eq. (7), contains two pairs of zero eigenvalues, one of which becomes finite (remaining stable, i.e., imaginary) at $C>0$. Our numerical findings, displayed in Fig. 2, reveal that, in compliance with the analytical results, the dipoles of both types give rise to virtually identical finite eigenvalues [hence only one eigenvalue line is actually seen in panel (d) of Fig. 2]. As shown in panel (e), both dipoles lose their stability simultaneously, at $C\approx 0.15$. Continuing the computations past this point, we conclude that the (unstable) vertical and horizontal dipoles become different when C attains values ~ 1. The unstable vertical configuration (B1) disappears through a saddle-node bifurcation at $C\approx 2.17$, while its horizontal counterpart (B2) persists through this point. Furthermore, there is a critical value of C at which an eigenvalue bifurcates from the edge of the continuous spectrum. Eventually, this eigenvalue crosses the origin of the spectral plane, giving rise to an additional unstable eigenvalue pair, with $\mathrm{Re}(\lambda)\neq 0$. The value of C at which this secondary instability sets in for (B1), $C\approx 1.55$, is essentially smaller than for (B2), which is $C\approx 2.61$.

Nonlinear evolution of unstable dipoles was examined in direct simulations as well. As seen in the example shown [for the configuration (B1)] in panels (f) of Fig. 2, the instability typically transforms them into fundamental solitons.

Proceeding to the lattice-soliton species (C), i.e., the horseshoe, we note that, because it is seeded at three sites in the ac limit, there are three pairs of zero eigenvalues at $C=0$. Above, it was shown analytically that one pair of these eigenvalues becomes finite at order $O(C)$ (being imaginary), and another at $O(C^2)$. These analytical results are continued by means of numerical computations, as shown in Fig. 3. It was found that the first pair remains stable (imaginary) until it collides with the edge of the continuous spectrum, which happens at $C\approx 0.25$ [see panels (d) and (e) of Fig. 3]. As mentioned above, the second eigenvalue pair, bifurcating from zero at order $O(C^2)$, is critical to the stability of the horseshoe at finite C. Numerical results show that this pair bifurcates into a *stable* one, hence, as shown in Fig. 3, the horseshoe remains stable up to the abovementioned value $C\approx 0.25$, at which the first pair suffers a bifurcation into an unstable one, due to the collision with the continuous band.

To understand the stabilizing effect of the surface on the horseshoes, it is relevant to compare them to their counterparts that may be found in the infinite lattice. Indeed, again starting with the ac seed taken as per Eq. (4) but far from the lattice's edge, we have created stationary structures similar to the horseshoe. By themselves, they present a family of localized solutions to the DNLS equation in 2D. However, this entire family turns out to be unstable (unlike the ordinary quadrupoles that may be stable in the infinite lattice [23]), through the following mechanism: the $O(C^2)$ eigenvalue pair, bifurcating from zero at $C=0$, immediately becomes real in this case, see the corresponding parabolic dashed-dotted line in panel (e) of Fig. 3. Thus, the presence of the

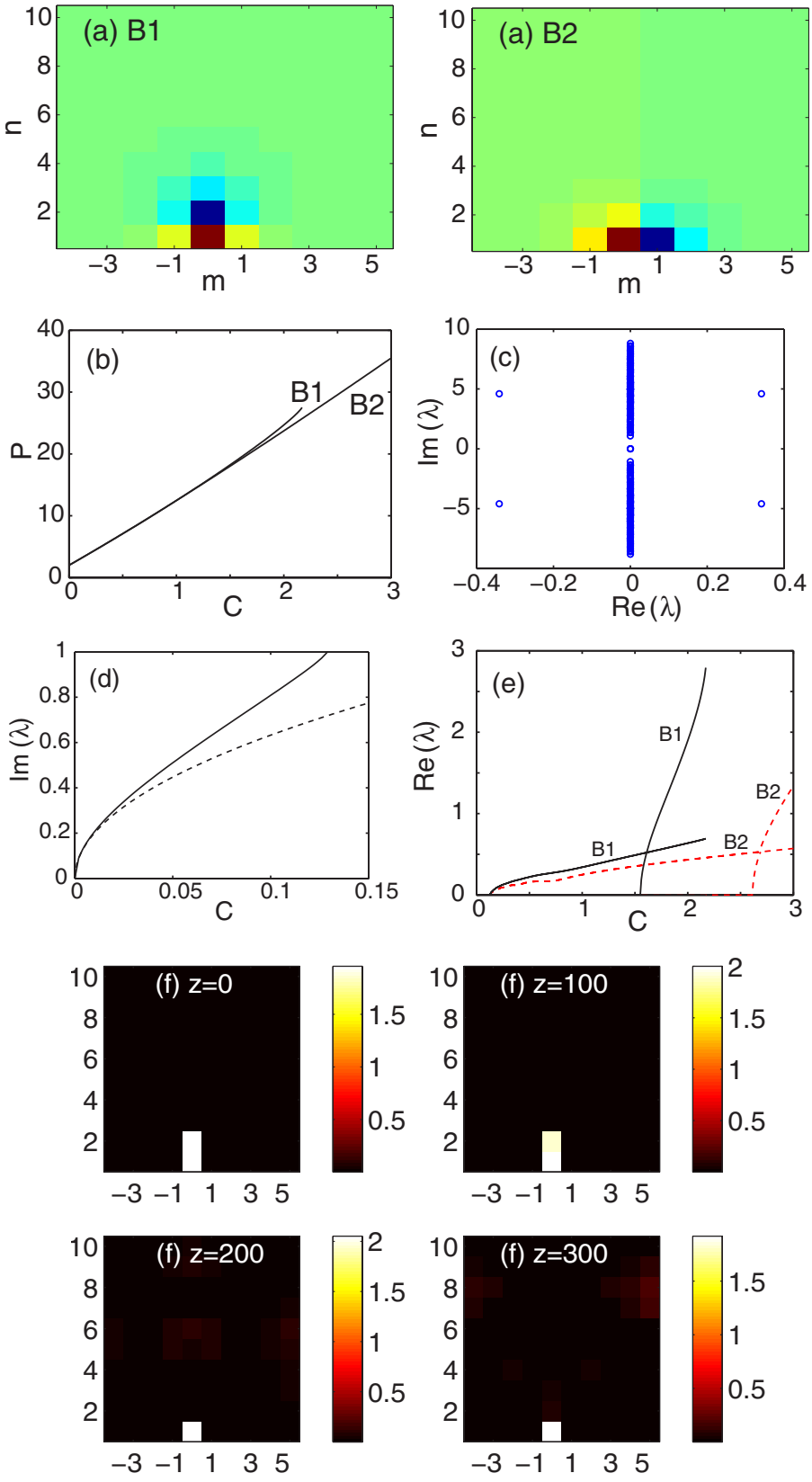

FIG. 2. (Color online) (a) Examples of vertical (B1) and horizontal (B2) dipoles for $C=1$. The norms of these solutions are depicted, versus the lattice coupling constant C in panel (b); panel (c) shows the spectrum of the stability eigenvalues for $C=0.2$. The imaginary and real parts of the critical stability eigenvalues are shown, as functions of C, in panels (d) and (e), respectively. The vertical dipole (B1) disappears via a saddle-node bifurcation at $C \approx 2.17$. Panel (d) depicts the eigenvalue bifurcating from zero at $C=0$, the dashed line being the analytical approximation described in the text, i.e., $[\mathrm{Im}(\lambda)]^2 = 4C$. Panel (e) shows the onset of instability of the (B1) (solid lines) and (B2) (dashed lines) dipoles, as found from numerical computations. Panels (f) show the nonlinear evolution of an unstable vertical dipole at $C=0.2$.

lattice edge is a crucial condition for the stability of the horseshoe patterns.

Panels (f) of Fig. 3 exemplify the evolution of the horseshoe when it is unstable. We observe that it splits into a pair of fundamental solitons, one trapped at the surface and one found deeper inside the lattice. In physical units, the propagation distances in the simulations of the instability evolution presented here are on the order of a few cm, which is certainly accessible to the current experiments (see, e.g., Refs. [26,20]).

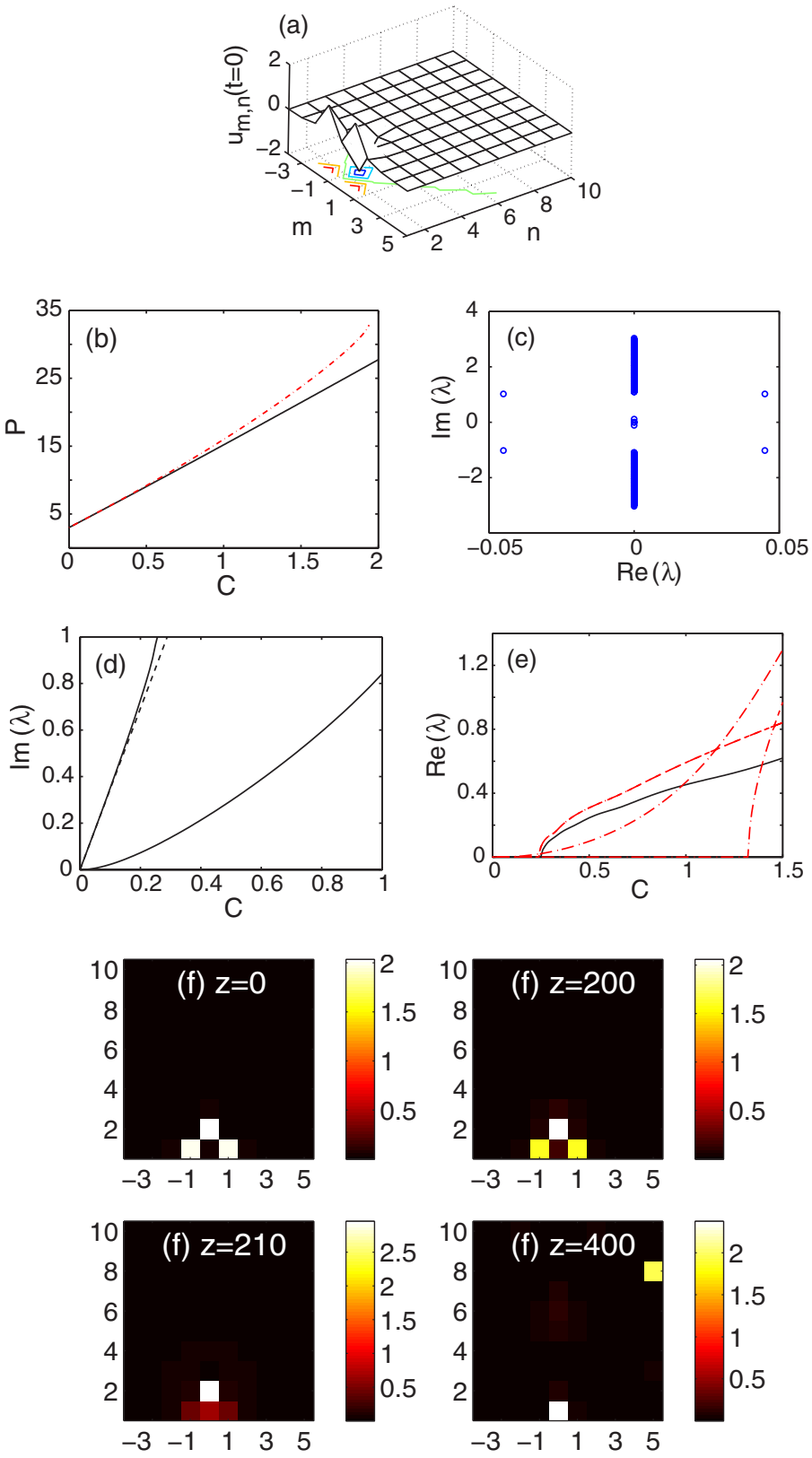

FIG. 3. (Color online) The same as Fig. 2 for the "horseshoe" configuration, seeded at $C=0$ as per Eq. (4) (i.e., as a truncated quadrupole). (a) Example of the pattern. The solid curves in panels (d) and (e) display the imaginary and real parts of critical stability eigenvalues [the dashed line in (d) presents the analytical approximation for the imaginary part, see text]. For comparison, the dash-dotted lines in (e) show the same characteristics for a family of horseshoe solitons created in the uniform lattice (without the edge). It is seen that the latter family is completely unstable, while the horseshoe trapped at the edge of the lattice has a well-defined stability region. Panels (c) and (f) present, respectively, the linear instability spectrum of the horseshoe at $C=0.26$, and its (numerically simulated) evolution due to the instability.

III. EFFECTS OF THE LATTICE SURFACE ON THE EXISTENCE OF VORTICES

In spite of the stabilization effects reported above, the lattice edge may also act in a different way, impeding the existence of localized solutions of other types. As an interesting example, we consider the so-called supersymmetric lattice vortex [19] attached to the edge, i.e., one with the vorticity ($S=1$) equal to the size of the square which seeds the vortex at $C=0$ (in the uniform lattice) through the following set of four excited sites, cf. Eq. (4):

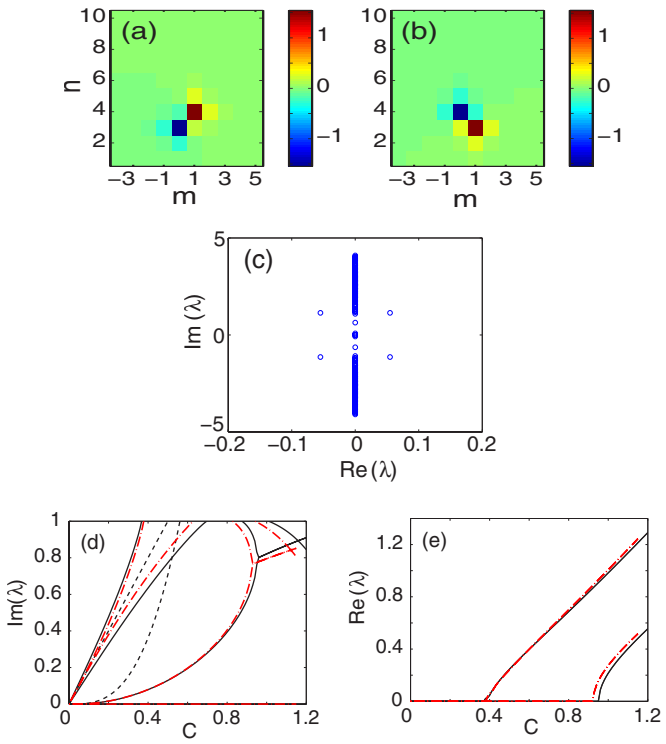

FIG. 4. (Color online) The supersymmetric vortex cell seeded as per Eq. (10). Panels (a) and (b) show, respectively, the real and imaginary parts of the solution, and panel (c) shows the (in)stability spectrum of small perturbations around it for $C=0.4$. Panels (d) and (e) display imaginary and real parts of the stability eigenvalues versus C. The solid and dashed lines show numerical and analytical results for small C. For comparison, dashed-dotted lines depict the same numerically found characteristics for a supersymmetric vortex on the infinite lattice.

$$\{v_{0,1}^{(0)},v_{1,1}^{(0)},v_{1,2}^{(0)},v_{0,2}^{(0)}\}=\{e^{i\theta_{0,1}},e^{i\theta_{1,1}},e^{i\theta_{1,2}},e^{i\theta_{0,2}}\}, \tag{9}$$

with $\theta_{0,1}=0$, $\theta_{1,1}=\pi/2$, $\theta_{1,2}=\pi$, and $\theta_{0,2}=3\pi/2$ (unlike the above configurations, this one is complex). While supersymmetric vortices exist in uniform lattices (including anisotropic ones), and have their stability regions [19,27], our numerical analysis has shown that the localized state seeded as per Eq. (9) in the model with the edge cannot be continued to $C>0$. In fact, we have found that, to create such a state at finite C, we need to seed it, at least, *two sites away* from the edge, i.e., as

$$\{v_{0,3}^{(0)},v_{1,3}^{(0)},v_{1,4}^{(0)},v_{0,4}^{(0)}\}=\{e^{i\theta_{0,3}},e^{i\theta_{1,3}},e^{i\theta_{1,4}},e^{i\theta_{0,4}}\}, \tag{10}$$

which is an accordingly translated version of Eq. (9). Numerically found stability eigenvalues for this structure are presented in Fig. 4, along with the analytical approximation, which was elaborated, for small C, by means of the same method as above. In all, there are four pairs of analytically predicted eigenvalues near the spectral-plane origin (given the four initially seeded sites of the configuration). More specifically, these are $\lambda=0$ (which corresponds to the Goldstone mode associated with the phase invariance), $\lambda=\pm 2iC$ (a double eigenvalue pair), and $\lambda=\pm\sqrt{32}C^3 i$ (a higher-order pair). As seen in the figure, the distance from the boundary equal to two lattice periods is sufficient to make the behavior of the supersymmetric lattice vortex sufficiently close to that in the infinite lattice, rendering the structure stable.

IV. CONCLUSION

This work demonstrates that properties of localized modes in the 2D lattice with an edge may be drastically different from well-known features in the uniform lattice. In particular, the edge expands the stability region of the fundamental solitons, and induces stability differences between dipoles oriented perpendicular and parallel to the lattice's border. On the other hand, an opposite trend was demonstrated regarding the existence of supersymmetric vortices, which cannot be created too close to the border. Most essentially, the edge stabilizes a new species of discrete solitons, the "horseshoe," which is unstable in the uniform lattice. The stabilizing effect exerted by the edge on the fundamental solitons, horizontal dipoles, and horseshoes suggests new possibilities for experiments in 2D arrays of nonlinear optical waveguides, as well as in BECs trapped in a deep 2D optical lattice. In particular, a straightforward estimate shows that the longest dimensionless propagation distance $z\lesssim 400$ (for which the simulations were run, to demonstrate the evolution of unstable modes in full detail and highlight their distinction from the stable ones), corresponds to a waveguide length $\lesssim 4$ cm, which is quite possible in the current experiments [20,26].

Natural issues for further consideration are horseshoes of a larger size (the present work was dealing with the most compact ones), and counterparts of such localized modes in 3D lattices near the edge—possibly, in the form of "bells" abutting on the surface. In the 3D lattice, one can also consider solitons in the form of vortex rings or cubes [28] set parallel to the border. In this connection, it is relevant to note that the 3D version of the DNLS equation does not apply to the guided-wave propagation in optics, but it can be realized in terms of BEC loaded in a strong 3D optical lattice (see, e.g., Ref. [28], and references therein).

ACKNOWLEDGMENTS

P.G.K. gratefully acknowledges support from Grant No. NSF-DMS-0204585, NSF-CAREER. R.C.G. and P.G.K. also acknowledge support from Grant No. NSF-DMS-0505663.

[1] R. K. Dodd, J. C. Eilbeck, J. D. Gibbon, and H. C. Morris, *Solitons and Nonlinear Wave Equations* (Academic Press, London, 1982).
[2] G. Maugin, *Nonlinear Waves in Elastic Crystals* (Oxford University Press, Oxford, 2000).
[3] L. Stenflo, Phys. Scr. **T63**, 59 (1996).
[4] K. G. Makris, S. Suntsov, D. N. Christodoulides, G. I. Stegeman, and A. Hache, Opt. Lett. **30**, 2466 (2005); M. I. Molina, R. A. Vicencio, and Y. S. Kivshar, Opt. Lett. **31**, 1693 (2006).
[5] S. Suntsov, K. G. Makris, D. N. Christodoulides, G. I. Stegeman, A. Haché, R. Morandotti, H. Yang, G. Salamo, and M. Sorel, Phys. Rev. Lett. **96**, 063901 (2006).
[6] E. Smirnov, M. Stepić, C. E. Rüter, D Kip, and V. Shandarov, Opt. Lett. **31**, 2338 (2006).
[7] M. I. Molina and Y. S. Kivshar, Phys. Lett. A **362**, 280 (2007).
[8] I. L. Garanovich, A. A. Sukhorukov, Y. S. Kivshar, and M. Molina, Opt. Express **14**, 4780 (2006).
[9] M. I. Molina, Phys. Rev. B **71**, 035404 (2005); **73**, 014204 (2006).
[10] Y. V. Kartashov, L. Torner, and V. A. Vysloukh, Phys. Rev. Lett. **96**, 073901 (2006); W. H. Chen, Y. J. He, and H. Z. Wang, Opt. Express **14**, 11271 (2006).
[11] C. R. Rosberg, D. N. Neshev, W. Krolikowski, A. Mitchell, R. A. Vicencio, M. I. Molina, and Y. S. Kivshar, Phys. Rev. Lett. **97**, 083901 (2006).
[12] G. A. Siviloglou, K. G. Makris, R. Iwanow, R. Schiek, D. N. Christodoulides, G. I. Stegeman, Y. Min, and W. Sohler, Opt. Express **14**, 5508 (2006).
[13] Y. V. Kartashov, A. A. Egorov, V. A. Vysloukh, and L. Torner, Opt. Express **14**, 4049 (2006).
[14] B. A. Malomed and P. G. Kevrekidis, Phys. Rev. E **64**, 026601 (2001).
[15] D. N. Neshev, T. J. Alexander, E. A. Ostrovskaya, Y. S. Kivshar, H. Martin, I. Makasyuk, and Z. Chen, Phys. Rev. Lett. **92**, 123903 (2004); J. W. Fleischer, G. Bartal, O. Cohen, O. Manela, M. Segev, J. Hudock, and D. N. Christodoulides, *ibid.* **92**, 123904 (2004).
[16] M. I. Molina, Phys. Rev. B **74**, 045412 (2006).
[17] Y. V. Kartashov (private communication).
[18] A. Trombettoni and A. Smerzi, Phys. Rev. Lett. **86**, 2353 (2001); G. L. Alfimov, P. G. Kevrekidis, V. V. Konotop, and M. Salerno, Phys. Rev. E **66**, 046608 (2002).
[19] D. E. Pelinovsky, P. G. Kevrekidis, and D. J. Frantzeskakis, Physica D **212**, 20 (2005).
[20] J. Meier, G. I. Stegeman, Y. Silberberg, R. Morandotti, and J. S. Aitchison, Phys. Rev. Lett. **93**, 093903 (2004); Y. Linzon, Y. Sivan, B. Malomed, M. Zaezjev, R. Morandotti, and S. Bar-Ad, *ibid.* **97**, 193901 (2006).
[21] P. G. Kevrekidis, B. A. Malomed, and A. R. Bishop, J. Phys. A **34**, 9615 (2001).
[22] J. Yang, I. Makasyuk, A. Bezryadina, and Z. G. Chen, Stud. Appl. Math. **113**, 389 (2004); Z. G. Chen, H. Martin, E. D. Eugenieva, J. J. Xu, and J. K. Yang, Opt. Express **13**, 1816 (2005).
[23] P. G. Kevrekidis, B. A. Malomed, Z. Chen, and D. J. Frantzeskakis, Phys. Rev. E **70**, 056612 (2004); H. Sakaguchi and B. A. Malomed, Europhys. Lett. **72**, 698 (2005).
[24] M. Johansson and S. Aubry, Phys. Rev. E **61**, 5864 (2000).
[25] N. Tzirakis and P. G. Kevrekidis, Math. Comput. Simul. **69**, 553 (2005).
[26] J. Meier, J. Hudock, D. Christodoulides, G. Stegeman, Y. Silberberg, R. Morandotti, and J. S. Aitchison, Phys. Rev. Lett. **91**, 143907 (2003).
[27] P. G. Kevrekidis, D. J. Frantzeskakis, R. Carretero-González, B. A. Malomed, and A. R. Bishop, Phys. Rev. E **72**, 046613 (2005).
[28] P. G. Kevrekidis, B. A. Malomed, D. J. Frantzeskakis, and R. Carretero-González, Phys. Rev. Lett. **93**, 080403 (2004); R. Carretero-González, P. G. Kevrekidis, B. A. Malomed, and D. J. Frantzeskakis, *ibid.* **94**, 203901 (2005).